Available online at www.sciencedirect.com
ScienceDirect
International Journal of Heat and Mass Transfer 50 (2007) 2656–2666
International Journal of HEAT and MASS TRANSFER
www.elsevier.com/locate/ijhmt

A numerical study of laminar free convection heat transfer between inner sphere and outer vertical cylinder

Wen Ruey Chen *

Department of Mechanical Engineering, Far East University, 49 Chung Hua Road, Hsin-Shih, Tainan Prefecture 744, Taiwan, ROC

Received 6 July 2006; received in revised form 22 November 2006

Abstract

The effects of height and radius ratio with a Newtonian fluid have been investigated numerically to determine heat transfer by natural convection between the sphere and vertical cylinder with isothermal boundary conditions. The inner sphere and outer vertical cylinder were heated and cooled in a steady change of temperature. Calculations were carried out systematically for a range of the Rayleigh numbers to determine the average Nusslet numbers which are affected by the geometric ratio parameters (*HR* and *RR*) on the flow and temperature fields. The governing equations, in terms of vorticity, stream function and temperature are expressed in a spherical polar coordinate system. Results of the parametric study conducted further reveal that the heat and flow fields are primarily dependent on the Rayleigh number and height and radius ratio, for a Prandtl number of 0.7, with the Rayleigh number ranging from 10^3 to 10^6, and the height and radius ratio varying from 1.2 to 5.0. Above all, the specification of different convective configurations has a significant effect on the average heat transfer rate across the composite annulus gap.

1. Introduction

The prices of petroleum keep going up at present. The requirement of the further energy always leans on the external energy surely, such as solar energy, wind-force, terrestrial heat, etc. The solar energy was the most extensively applied among them because of its importance in the thermal storage systems of the solar energy collectors. In particular, the problems of buoyancy-driven flow in enclosed spaces are being investigated most extensively; hence the natural convection heat transfer in the annulus between two concentric and eccentric cylinders, and that in the annulus between two concentric and vertically eccentric spheres have received considerable attention from researchers in many diverse fields of applications. Such problems commonly occur within the geophysical fields, cooling of electronic equipment, aircraft cabin insulation, solar energy collectors, thermal storage systems as well as nuclear reactor design, and many other practical situations. As a result, extensive experimental and theoretical works deal with flow and associated heat transfer characteristics of natural convection in annuli between two isothermal horizontal concentric and eccentric cylinders [1–7]. Experimental research on natural convection in annuli between two isothermal concentric spheres has been described in Refs. [8–10]. The flow patterns in the annuli between the concentric spheres were observed for various radius ratios, Prandtl numbers, and Rayleigh numbers. These were crescent eddies, kidney-shaped flows, and falling-vortices. Using the numerical analysis investigate steady state laminar free convection in annuli between two isothermal concentric spheres in Refs. [11–14] have been reported in the literature. Other solutions of the problem which deal with transient natural convection in the same geometric structure with uniform wall temperatures have been made in Refs. [15–20]. Further understanding of the different geometric structure in a steady state and transient convective heat transfer phenomena is essential to design and operation of

* Tel.: +886 6 5977051; fax: +886 6 5977050.
E-mail address: ruey666@cc.feu.edu.tw

0017-9310/$ - see front matter © 2007 Elsevier Ltd. All rights reserved.
doi:10.1016/j.ijheatmasstransfer.2006.11.046

Nomenclature

C_p	specific heat at constant pressure
g	local gravitational acceleration
h	heat transfer coefficient
H	dimensionless height of the vertical cylinder
$\overline{H}$	height of the vertical cylinder
HR	height ratio H/r_s
k	thermal conductivity
L	gap, $\sqrt{\overline{H}^2+\bar{r}_c^2}-\bar{r}_s$
Nu	local Nusselt number, hL/k
$(\overline{Nu})$	average Nusselt number, hL/k
P, Q	function used in coordinate transformation
Pr	Prandtl number, v/α
R	dimensionless radial coordinate, $\bar{r}/L$
$\bar{r}$	radial coordinate
R	dimensionless radial profile of outer cylinder, $\overline{R}/L$
$\overline{R}$	radial profile of outer cylinder
Ra	Rayleigh number, $g\beta\Delta\overline{T}L^3/v\alpha$
RR	radius ratio, r_c/r_s
T	dimensionless temperature, $(\overline{T}-\overline{T}_c)/(\overline{T}_s-\overline{T}_c)$
$\overline{T}$	temperature
v	velocity
V	dimensionless velocity, vL/α

Greek symbols

α	thermal diffusivity
β	thermal expansion coefficient
$\Delta\overline{T}$	temperature difference between spheres, $\overline{T}_s-\overline{T}_c$
η	dimensionless radial coordinate in transformed plane, $(r-r_s)/(R-r_s)$
ξ	dimensionless angular coordinate in a spherical system, θ/π
θ	angular coordinate in a spherical system
α^*, β^*, γ^*	factor of coordinate transformation
θ^*	angular position at vortex center
μ	dynamic viscosity
v	kinematic viscosity, μ/ρ
ρ	fluid density
v^*, v^*	factor of coordinate transformation
φ	azimuthal coordinate in a spherical system
ψ	dimensionless stream function, $\bar{\psi}/\alpha L$
$\bar{\psi}$	stream function in spherical coordinates
ω	dimensionless vorticity, $\bar{\omega}L^2/\alpha$
$\bar{\omega}$	vorticity

Subscripts

c, s	cylinder and sphere
d	diagonal
m	mean
max	maximum

various engineering application of thermal fluid systems, such as solar energy collectors and energy systems including nuclear reactors. This would be the reason for the fact that studies on natural convection between concentric and vertically eccentric spheres have increased recently [21–23]. A numerical solution for geometric shape between concentric and vertically eccentric spheres of various radius ratio with a large range of Rayleigh number $Ra = 10^3$–5×10^5 has been computed. However, most of the studies are concerned with the concentric or vertically eccentric spheres of the problems, thus knowledge about thermal convection with other combination of the different geometric shape [24–27] is limited in thermal science field.

To further extend the existing knowledge on natural convection heat transfer of Newtonian fluids in the thermal engineering, the author is motivated by interest in demonstrating the effects of a height and radius ratio as well as buoyancy in the laminar free convection flow between sphere and vertically cylinder with constant temperature boundary conditions. A finite difference solution is obtained for the governing equations in terms of stream function, vorticity, energy in a spherical coordinate system. The effects of geometric structure, Rayleigh number, and fluid property on the flow fields and heat transfer characteristics are discussed, respectively. The details of the method are described in the next section. We wish to point out that our formulations were represented by general form for various natural convection problems involving in the annuli combined with inner sphere and outer vertically cylinder.

2. Mathematical formulation

The geometric configuration of the physical system is a composite annulus which consists of the inner sphere and vertical cylinder. It is the arrangement of circular cylinder of radius r_c with height h, which contain a circular sphere of radius r_s and the common origin of the coordinates located at O. The height ratio is repressed by HR which is ratio of cylindrical height to spherical radius, and the RR is defined by radius ratio which is the ratio of the radius of the cylinder to sphere. For a natural convective heat transfer problem, the largest heat transfer variation due to values of HR and RR occurs when the direction of cylindrical height is aligned with the gravitational direction. Therefore, this study focuses on the problem that HR and RR are vertically and horizontally shifted, respectively.

The space between the inner sphere and outer vertical cylinder is filled with a viscous and incompressible Newtonian fluid. Initially, the annuli are at a uniform temperature T_c, and a quiescent state is assumed, while the inner sphere

is heated with a constant temperature T_s and the outer vertical cylinder surface with top and bottom surface is cooled at a fixed temperature T_c. The heat transfer takes place in the annuli by natural convection. A model to describe the process has been derived with the following assumptions: (1) the flow within the annulus is laminar, (2) all fluid properties, are taken to be constant, except for the density variation with temperature in the buoyancy term, i.e. the Boussinesq approximation is valid, (3) the flow is symmetrical about the vertical axis which is parallel to the line of gravity acceleration, and (4) viscous dissipation and radiation effects are neglected.

A spherical coordinate system (r, θ, φ) and grids system were chosen as shown in Fig. 1. The angle $\theta = 0°$ is defined on the top surface of the cylinder and $\theta = 180°$ is defined beneath the bottom surface of the cylinder. To deal with the numerical formulation associated with the complex physical domain of the annulus between sphere and vertical cylinder, a radial coordinate transformation is adopted to map the cylinder-sphere annular gap into a unit sphere. The surface of outer cylinder $r = R(\theta)$ [28] is transformed into the unit sphere $\eta = 1$, while the inner sphere radius $r = r_s$ is transformed into the pole $\eta = 0$. This transformation is obtained by defining a new radial coordinate as

$$\begin{cases} \eta = \frac{r - r_s}{R(\theta) - r_s} \quad (1.1) \\ \xi = \frac{\theta}{\pi} \quad (1.2) \end{cases} \tag{1}$$

where $R(\theta)$ denotes variable dimensionless profile of the outer cylinder surface measured from the center of the inner sphere, which is symmetric with respect to the vertical axis in any angular position of φ-direction and is expressed by

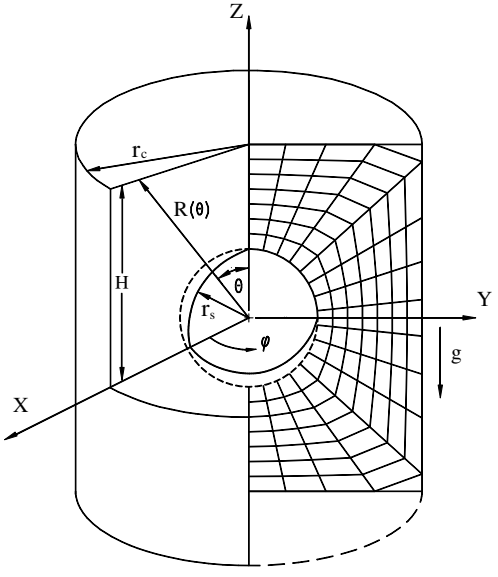

Fig. 1. Coordinate and grids system for annulus between sphere and vertical cylinder.

$$R(\theta) = \begin{cases} H \sec\theta & 0 \leqslant \theta < \theta_d \\ r_c \csc\theta & \theta_d \leqslant \theta < (\pi - \theta_d) \\ -H \sec\theta & (\pi - \theta_d) \leqslant \theta < \pi \end{cases} \tag{2}$$

The governing equations for the two-dimensional problem in dimensionless terms can be written as follows:

Vorticity transport equation:

$$\frac{1}{r^2 \sin\theta}\left\{\lambda^*[\psi_\xi \omega_\eta - \psi_\eta \omega_\xi] + [v^* \psi_\eta + v^* \psi_\xi]\omega\right\} = Pr\left[\nabla_1^2 - \frac{1}{r^2 \sin^2\theta}\right]\omega - Pr \cdot Ra\left[\left(\eta_r \sin\theta + \eta_\theta \frac{\cos\theta}{r}\right) T_v + \left(\epsilon_r \sin\theta + \epsilon_\theta \frac{\cos\theta}{r}\right) T_\xi\right] \tag{3}$$

Stream function equation:

$$D_1^2 \psi = \omega r \sin\theta \tag{4}$$

Energy equation:

$$\frac{1}{r^2 \sin\theta}\left[\lambda^*(\psi_v T\xi - \psi_\xi T_v)\right] = \nabla_1^2 T \tag{5}$$

where

$$\nabla_1^2 = \left[P\frac{\partial}{\partial\eta} + Q\frac{\partial}{\partial\xi} + \alpha^*\frac{\partial^2}{\partial\eta^2} + 2\gamma^*\frac{\partial^2}{\partial\eta}\partial\xi + \beta^*\frac{\partial^2}{\partial\xi^2}\right] \tag{6}$$

$$D_1^2 = \alpha^*\frac{\partial^2}{\partial\eta^2} + \gamma^*\frac{\partial^2}{\partial\eta\partial\theta} + \beta^*\frac{\partial^2}{\partial\theta^2} + \left(A - \frac{\cot\theta}{r^2}\eta_\theta\right)\frac{\partial}{\partial\eta} - \left(C - \frac{\cot\theta}{r^2}\xi_\theta\right)\frac{\partial}{\partial\theta} \tag{7}$$

$$\begin{cases} P = A + \frac{2}{r}\eta_r + \frac{\cot\theta}{r^2}\eta_\theta \quad (8.1) \\ Q = C + \frac{2}{r}\xi_r + \frac{\cot\theta}{r^2}\xi_\theta \quad (8.2) \end{cases} \tag{8}$$

$$\begin{cases} A = \eta_{rr} + \frac{1}{r^2}\eta_{\theta\theta} \quad (9.1) \\ C = \xi_{rr} + \frac{1}{r^2}\xi_{\theta\theta} \quad (9.2) \end{cases} \tag{9}$$

$$\begin{cases} \alpha^* = \eta_r^2 + \frac{1}{r^2}\eta_\theta^2 \quad (10.1) \\ \beta^* = \xi_r^2 + \frac{1}{r^2}\xi_\theta^2 \quad (10.2) \\ \gamma^* = \eta_r\xi_r + \eta_\theta\xi_\theta \quad (10.3) \end{cases} \tag{10}$$

$$\begin{cases} \lambda^* = \eta_r\xi_\theta - \eta_\theta\xi_r \quad (11.1) \\ v^* = \frac{\eta_\theta}{r} - \eta_r\cot\theta \quad (11.2) \\ v^* = \frac{\xi_\theta}{r} - \xi_r\cot\theta \quad (11.3) \end{cases} \tag{11}$$

The associated boundary conditions for the problem considered are as follows:

At $\eta = 0$:

$$\psi = \psi\eta = 0, \quad T = 1, \quad \omega = \frac{1}{r_s \sin\theta}\alpha^*\psi_{\eta\eta},$$
$$N = \frac{1}{2}\omega \tag{12}$$

At $\eta = 1$:

$$\psi = \psi_\eta = 0, \quad T = 0, \quad \omega = \frac{1}{R\sin\theta}\alpha^*\psi_{\eta\eta}, \quad N = \frac{1}{2}\omega \tag{13}$$

At $\xi = 0$, 1:

$$\psi = \omega = N = T_\theta = 0 \tag{14}$$

From the above formulation, the governing parameters for the present problem are the Rayleigh number Ra, the Prandtl number Pr, the height and radius ratio are HR and RR, respectively.

The local and average Nusselt number at inner sphere and outer vertical cylinder surface are defined as:

$$Nu_{s,c} = -\left(\frac{1}{R} - \frac{1}{r_s}\right)\left[r^2\eta_r T_\eta\right]_{\eta=0,1} \tag{15}$$

$$\overline{Nu} = -\pi\int_0^1 Nu_{s,c}\left[\frac{\sin\theta}{2}\right]d\theta \tag{16}$$

3. Numerical method

From the above formulation, the parameters of governing equations are thus the Rayleigh number Ra, the Prandtl number Pr, the height ratio HR, and the radius ratio RR. To solve the present problem, the governing equations as well as boundary conditions were discritized by the finite difference method. Eqs. (3)–(5) expressing the vorticity transport, stream function, and energy transport equations, together with boundary conditions in Eqs. (12)–(14), provide a complete description of the problem. In this study, the finite difference equations were derived by using central difference approximations for the partial derivatives except the convective terms for which a quadratic upwind difference formula was employed. Derivative at the boundaries were approximated by a three point forward or backward difference. The equations of temperature, angular momentum and vorticity were solved by successive line relaxation method [29], while the stream function equation was solved by the modified strongly implicit procedure (MSIP) [30]. The solution was considered convergent when the relative error between the new and old values of the field variables Φ was less than a prescribed criterion (10^{-4}), where Φ represents ω, ψ and T

$$\frac{|\Phi_{new} - \Phi_{old}|_{max}}{|\Phi_{new}|_{max}} \leqslant 10^{-4}. \tag{17}$$

4. Results and discussion

The results of the numerical calculation have been performed systematically for a Newtonian fluid of the Prandtl number fixed at 0.7, The Rayleigh numbers ranging from 10^3 to 1.0×10^6, the height and radius ratio varying from 1.2 to 5.0. To see the effect of mesh size on the numerical result, computations for an annulus were carried out using seven different mesh sizes. The resulting Nusselt numbers are presented in Fig. 2. The local Nusselt numbers, obtained from seven different mesh sizes, are similar to each other, except that the local value of outer sphere at $\theta = 0°$ and $\theta = 35°$ are sensitive to the nodding size, and the result seems to converge at 52×52. In order to solve the computation effort, the results presented in this article are all obtained by using the grid size of 52×52. Numerical test calculations were also performed for different grid sizes. Two different grid sizes depending on the HR, RR and Ra have been used for the calculations: 52 (radial direction) by 52 (angular direction) for range of $1.2 \leqslant HR$ and $RR \leqslant 5.0$ within range of $1.0 \times 10^3 \leqslant Ra \leqslant 1.0 \times 10^5$, 62 by 62 for range of $1.4 \leqslant HR$ and $RR \leqslant 5.0$ with $Ra = 1.0 \times 10^6$. The maximum Rayleigh number was limited by numerical convergence, which in turn was dependent on the radius ratio. The limit of the Rayleigh number is 10^6 for the height and radius ratio of 1.2. The computations were performed on a personal computer (Intel (R) Pentium (R) D CPU 3.20 GHz) and required two different CPU time are 339 and 567 s for 52×52 and 62×62 grid systems, respectively.

Fig. 3 shows a distribution of streamlines and isotherms at fixed height and radius ratio of 1.2, i.e., $HR = RR = 1.2$, and Prandtl number of 0.7, for a series Rayleigh number of $Ra = 10^3$, 10^4, and 10^5, respectively. This series of results is designed to show the individual influence of height and radius ratio for the heat and flow fields. Because the problem is symmetric to the vertical axis, each annulus contains

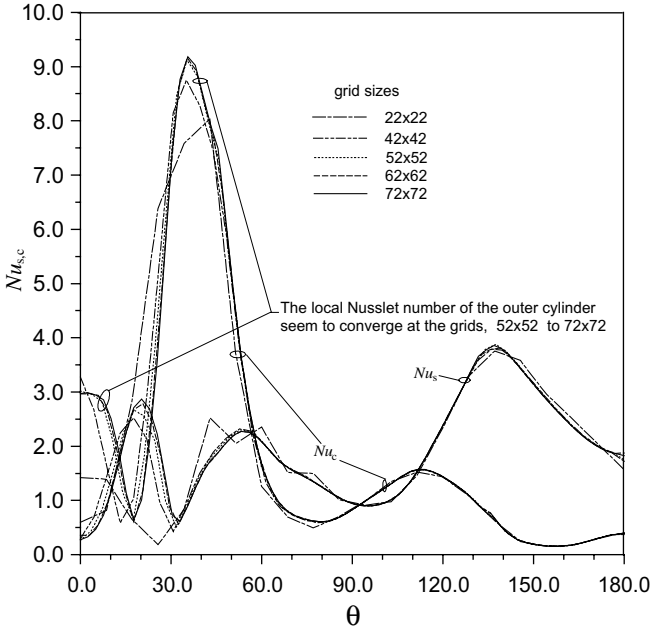

Fig. 2. Comparison of the local Nusselt number at the different grid sizes for $Pr = 0.7$, $Ra = 10^5$ and $HR = RR = 1.2$.

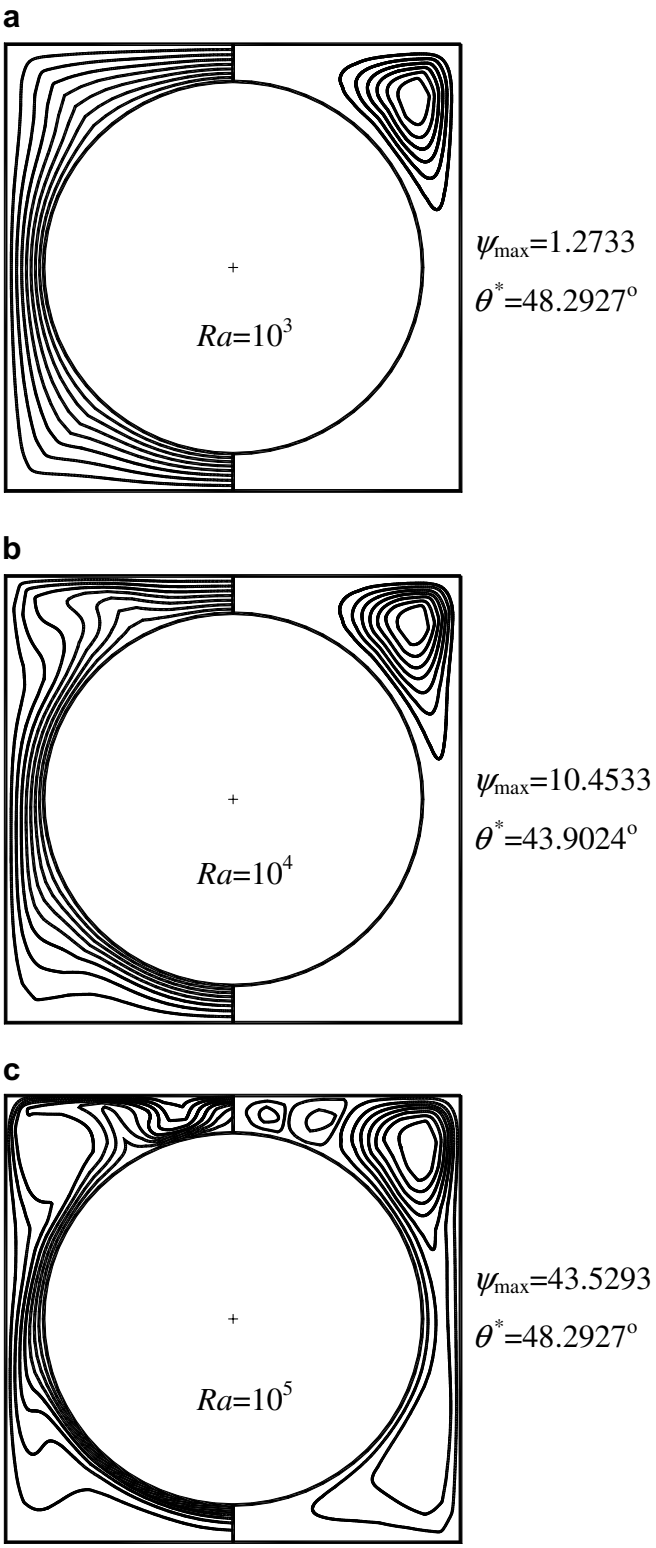

Fig. 3. Streamline (right) and isotherms (left) for $HR = RR = 1.2$: (a) $Ra = 10^3$; (b) $Ra = 10^4$; and (c) $Ra = 10^5$.

the isotherms on the left and streamlines on the right. Their number of contours within geometry is kept constant at eight for isothermal and streamline. Since the inner sphere is kept hotter, the hot fluid near the surface of the inner sphere rises upward due to thermal expansion. The uprising plume is then cooled down by the colder fluid near the upper part of the surface of the outer cylinder. The colder and denser fluid will eventually flow downward along the surface of the outer cylinder. For the conditions selected in the Rayleigh number of 1000, the maximum value of stream function $\psi_{max} = 1.2733$ lies at $\theta = 43.9024°$ from the upper vertical line of symmetry and at about the midgap position. At this Rayleigh number, the fluid flow in the half-annulus is weak and forms a vertical axial symmetrical recirculation in the clockwise direction, making the streamline patterns are located on a near corner of the upper cylinder. The isotherms are nearly circular, further indicating little influence of the convective flow on heat transfer conduction was the dominant mode of heat transfer. The center of the triangular-shaped eddy stayed close to midgap as variables were changed, but moved into the upper midgap as the Rayleigh number increased. When the case of $Ra = 10^5$, the vortex center (the position with the maximum value of the stream function) falls to the upper portion and dips near the $\theta = 48.2927°$ position when the height and radius ratio is reduced, the counterclockwise rotating secondary cell in the top of the midgap while the primary central eddy is clockwise. Even though the third cell appears near the vertically symmetric axis, it rotates clockwise and is weak while the secondary vortex rotates anti-clockwise. Though the geometry provides a least favorable circumstance for the development of natural convection, the narrow gap regions of the upper and bottom was essentially convective flow with high velocities. The laminar convection was the dominant mode of heat transfer. It is revealed that the isotherms are an inversion and streamlines are twin-triangular eddy-shaped. Finally, the maximum value of stream function is $\psi_{max} = 43.5293$.

Fig. 4 presents a series of streamline configurations and isotherm distributions for various combinations of $Pr = 0.7$; $Ra = 10^3$, 10^4 and 10^5 and $HR = RR = 2.0$. When compared with Figs. 3–5 show that at fixed Rayleigh number, as the height and radius ratio increases with decrease in the maximum value of the stream function. It is revealed that the source of the buoyancy-driven flow [31] mainly coming from the inner spherical surface because the surface has greater contact area of the heat transfer with respect to the smaller value of HR and RR. So that it has greater buoyancy that drives the fluid flow, making the fluid with high velocity flow within this narrow gap. Common to the results displayed for the three geometries (i.e., $HR = RR = 1.2$, 2.0 and 5.0) is that as the Rayleigh number increases, the maximum value of the stream function increases, indicative of a higher rate of heat convection due to the stronger buoyancy flow in the gap. The height and radius ratios of 1.2 and 5.0 cases are shown in Figs. 3 and 5. As expected, as the Rayleigh number increases, the vortex center rises to the upper portion except that the secondary cell is formed in this narrow region and possessed of upper portion; the primary clockwise cell is dips near the $\theta = 48.2927°$ as shown in Fig. 3 when the Rayleigh number is 10^5. Surprisingly, the

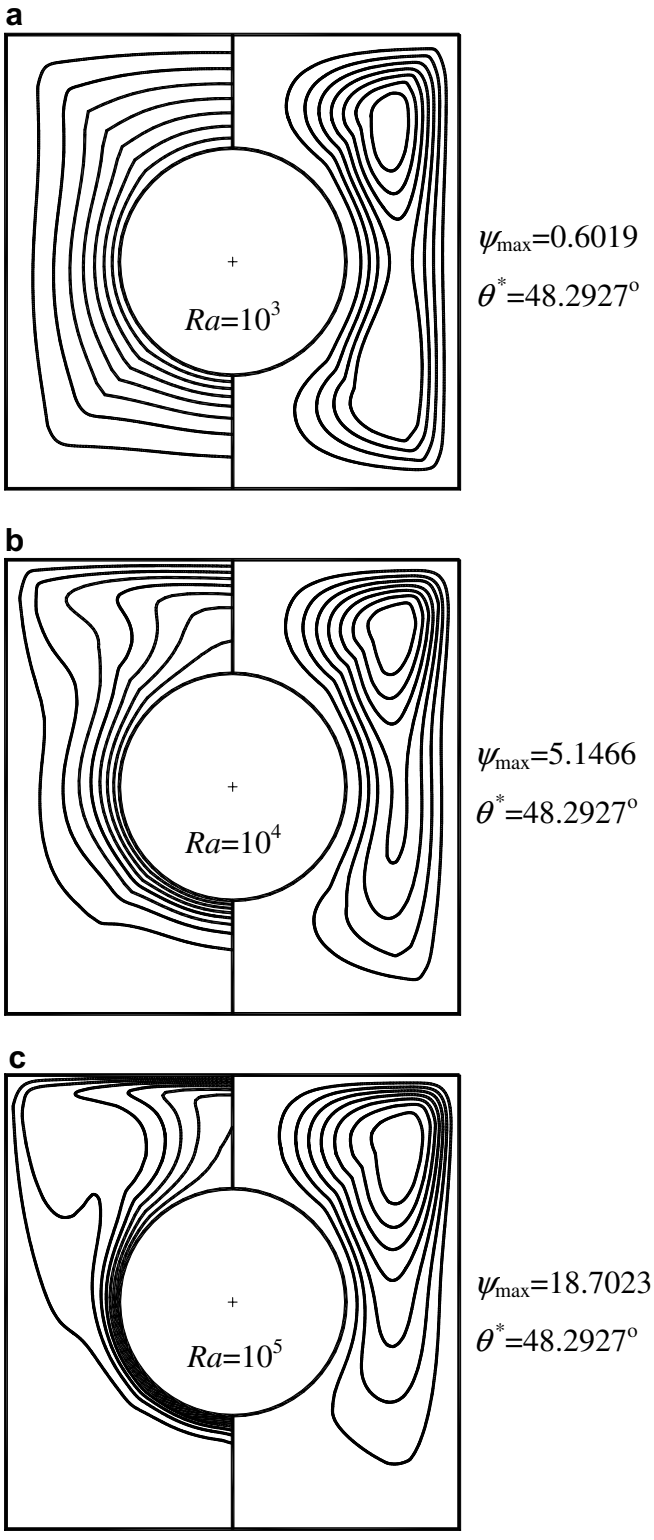

Fig. 4. Streamline (right) and isotherms (left) for $HR = RR = 2.0$: (a) $Ra = 10^3$; (b) $Ra = 10^4$; and (c) $Ra = 10^5$.

height and radius ratio is 2.0, as shown in Fig. 4. It is evident that the maximum value of stream function increases with increasing the Rayleigh number but the position of the vortex center always stays on the upper portion at the position

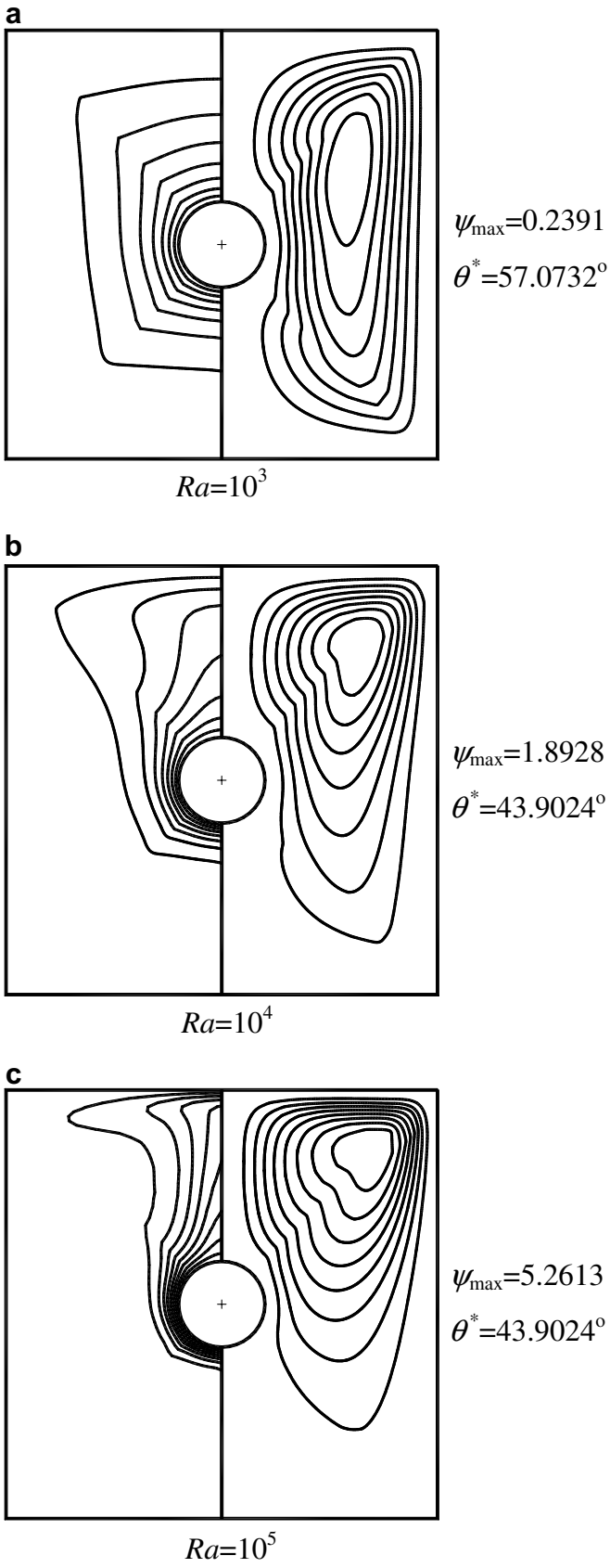

Fig. 5. Streamline (right) and isotherms (left) for $HR = RR$=5.0: (a) $Ra = 10^3$; (b) $Ra = 10^4$; and (c) $Ra = 10^5$.

of $\theta = 48.2927°$. It appears that the fluid within such favorable configuration for convective motion can be provided with both timely and favorable heat transfer convective environment.

Fig. 5 shows a larger value of height and radius ratio, i.e., $HR = RR = 5$. This geometric expressed that the fluid in the inner spherical surface for the convection contact area is relatively smaller than that of the outer cylindrical surface. It examines that the main power source of the fluid flow near the inner spherical surface with respect to the convection contact area is relatively smaller than those corresponding to the other values of $HR = RR = 1.2$ and 2.0. Since, the total heat flux from inner spherical surface to the outer cylindrical surface is relatively reduced under the same situation of the Rayleigh number. Even though the fluid within the spacious configuration should have a favorable convection, the buoyancy-driven flow is weak. However, within such favorable configuration for convective motion, as Ra increases, i.e., the value of Ra from 10^3 to 10^5, the fluids motion becomes stronger; the position of vortex center of the eddy shifts upward, first moving upward and then slowly moving upward, finally staying at the angular position of $\theta = 43.9024°$ (from the upper vertical line symmetry about midgap position) while the maximum value of stream function $\psi_{max} = 5.2613$.

The local and average Nusselt numbers for the inner sphere and outer vertical cylinder were defined as in Eqs. (15) and (16). Basically, an average Nusselt number of unity expresses pure conduction heat transfer and an average Nusselt number larger than unity indicates the enhancement of heat transfer by free convection instead of the pure conduction heat transfer. The variation of local Nusselt number on the inner sphere and outer vertical cylinder at $Pr = 0.7$, $HR = RR = 1.2$ with different Rayleigh number are $Ra = 10^3$, 10^4 and 10^5 is shown in Fig. 6. It is interesting to investigate the influence of various Rayleigh numbers on the thermal transport of the gap. It can be shown that the local Nusselt number distributes on the inner sphere and outer vertical cylinder with the Newtonian fluid. In this geometric, i.e., $HR = RR = 1.2$, when the Rayleigh number increases, the laminar convection is dominant mode of the heat transfer and multi-cell is gradually formed in the upper narrow portion of the annuli. It is apparent that the some peak values of the local Nusselt number are located on the outer cylindrical surface between the primary flow and the secondary flow in the narrow gap. It implies that the fluid flow into the wall has a maximum impulse normal to the wall, where is just stagnant flow forward on the surface. On the other hand, the fluid flow to be distant from the wall where has a minimum impulse normal to the wall, and is sometimes called stagnant flow backward on the surface. When the Rayleigh number is $Ra = 10^5$, it is remarkable that the maximum local Nusselt number on the outer vertical cylinder (Nu_c) and the minimum local Nusselt number (Nu_s) on the inner sphere are located on the angular position of $\theta = 35°$ and 31°, respectively, just between primary cell and secondary cell. Therefore, the maximum stream function of the primary cell is both larger and stronger than those for the lower Rayleigh number; the streamlines are depicted in the larger feature and have multi-cell while the isothermals exhibit to have multi-inversion.

Fig. 7 presents a series of local Nusselt number distribution on the inner sphere and outer vertical cylinder for height and radius ratio of 2.0 and Prandtl number of 0.7 with various Rayleigh numbers. For the specified heat flux on the wall, the surface Nusselt number is one of the important variables in the present calculations, since it

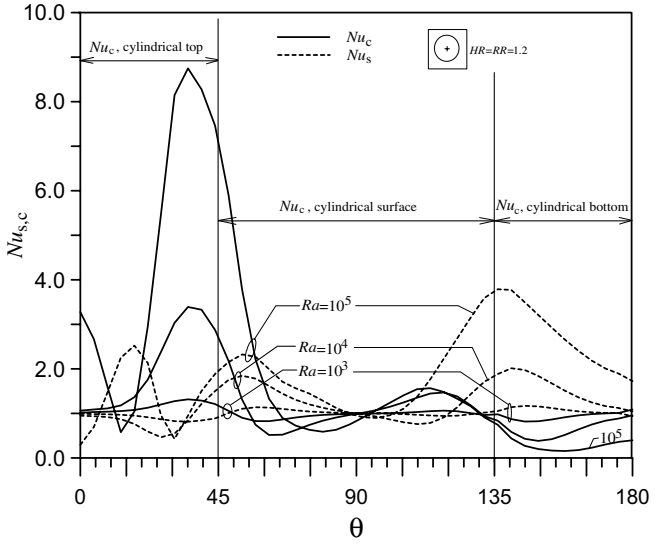

Fig. 6. The variation of local Nusselt number on the inner sphere and outer vertical cylinder for $HR = RR = 1.2$, $Pr = 0.7$ and $Ra = 10^3$, 10^4 and 10^5.

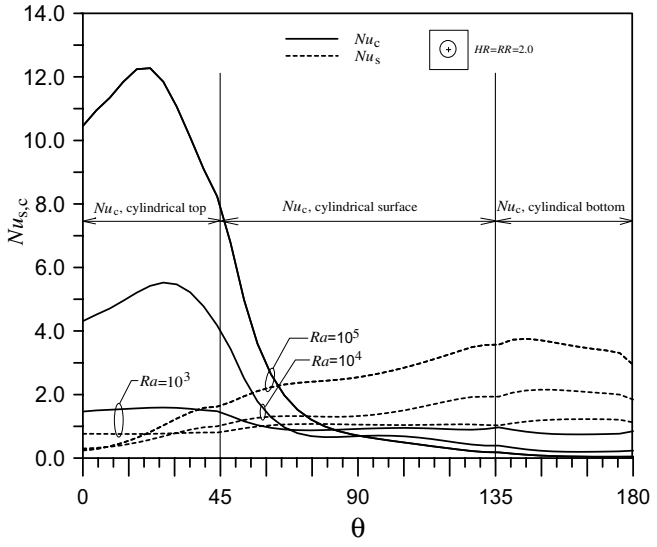

Fig. 7. The variation of local Nusselt number on the inner sphere and outer vertical cylinder for $HR = RR = 1.2$, $Pr = 0.7$ and $Ra = 10^3$, 10^4 and 10^5.

can reflect the local heat transfer characteristics along the solid surface. The circumferential Nusselt number distribution along the solid surface is at various Ra. Common to the results displayed for this geometry ($HR = RR = 2.0$) is that as the Rayleigh number increases, the local Nusselt number (Nu_c) of the outer vertical cylinder has some clearer peak values of the Nu_c that increases between the angular position $\theta = 20°$ and 25° near the upper outer vertical cylinder surface, while Nu_c decreases relatively at $\theta = 135$–150° near the bottom of the outer cylinder. It indicates that the peak value with a higher rate of heat transfer was due to the stronger buoyancy flow into the solid surface in the upper portion, while the mitigating value with a lower rate of heat transfer in the bottom was essentially stagnation with low velocities. For the local Nusselt number distribution on the inner sphere (Nu_s) increases slowly with increasing Rayleigh number (Ra), which is distributed on the major portion of the bottom of the sphere with middle convection mode. But the heat transfer with conduction mode is distributed on the minor portion of the top of the sphere.

Fig. 8 shows the local Nusselt number distribution on the inner sphere and outer vertical cylinder for height and radius ratios of 5.0 and Prandtl number of 0.7 with various Rayleigh numbers (Ra). As Rayleigh number increases, the peak values of the Nu_c always occur near the top of the cylinder and the nadir values of the Nu_s always stays near the top of sphere in the axis of vertical symmetric at $\theta = 0°$ for all Rayleigh numbers, where the fluid upflows mainly along the radial and vertical direction, but there is minor angular velocity. It is apparent that the maximum local Nusselt number (Nu_c) on the top surface of cylinder belongs to a laminar free convection and the minimum local Nusselt number (Nu_s) on the top surface of the sphere seems to be into a pure conduction. On the contrary, as the fluid moves downward, it loses energy and

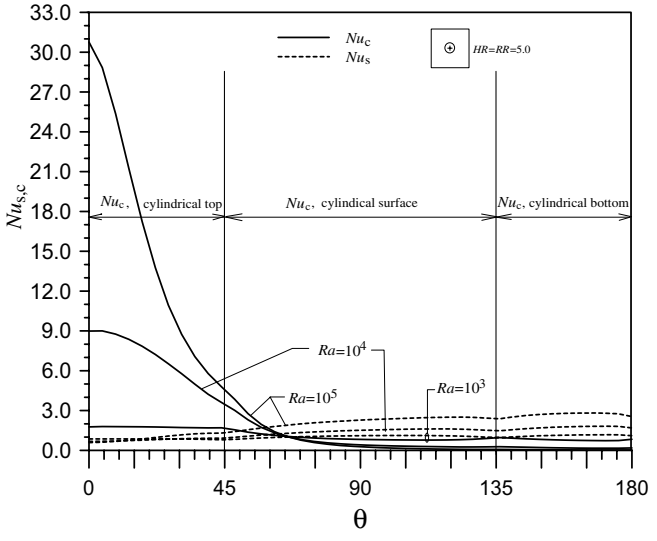

Fig. 8. The variation of local Nusselt number on the inner sphere and outer vertical cylinder for $HR = RR = 1.2$, $Pr = 0.7$ and $Ra = 10^3$, 10^4 and 10^5.

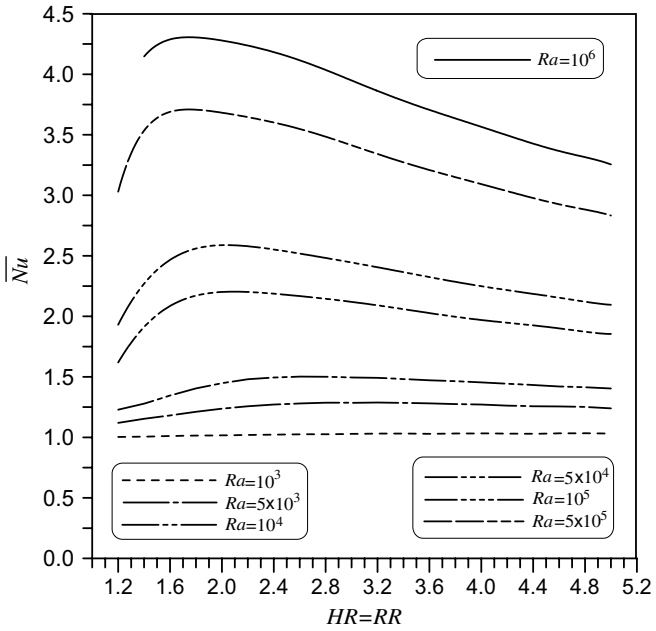

Fig. 9. Average Nusslet number as function of the height and radius ratio for $Pr = 0.7$ at various different Rayleigh numbers.

eventually forces the separation of the thermal boundary layer along the outer cylinder. The heavy fluid then enters the thermal boundary layer of the inner sphere and completes the recirculation pattern. When the bottom of the annulus in the axis of vertical symmetric is near $\theta = 180°$, where the fluid upflows on the bottom inner sphere surface with moderate convective heat transfer mode while upflows to leave the bottom outer cylinder surface with lower conduction heat transfer mode. We also find that the $Nu_{c,s}$ between $\theta = 60°$ and 180° are smaller and milder, which implies that the local heat flux at both inner sphere and outer vertical cylinder should be almost independent of θ.

Fig. 9 shows the average Nusselt number $\overline{Nu}$ varies with height and radius ratio (HR and RR) under the various fixed values of $Ra = 10^3$, 5.0×10^3, 10^4, 5.0×10^4, 10^5, 5×10^5 and 10^6, respectively. It can be observed that each convex curve that has a maximum of the heat transfer, which arises within the range $1.6 \leqslant HR = RR \leqslant 3.4$ depending primarily on the Rayleigh number. This is due to the presence of optimum geometric convective space under the same magnitude of Rayleigh number, i.e., the same effect of buoyancy. The occurrence of maximum heat transfer signifies onset of a regime where the decrease in the conduction with corresponding to the height and radius ratio (HR and RR) is enough to offset the increase in convection. When the Ra is fixed at 10^3, the maximum average Nusselt number ($\overline{Nu}$) is 1.03188 as $HR = RR = 3.4$ which is best convective space relative to the other values of $HR = RR$. The maximum Nusselt number ($\overline{Nu}$) versus corresponding to the value of the height and radius ratio (HR and RR) with various different Rayleigh number is displayed in Table 1. At fixed Rayleigh numbers, the average Nusselt number always increases fast with increasing the height and radius ratio initially until when the maximum

Table 1
Maximum average Nusselt number with respect to the height and radius ratio under various different Rayleigh numbers

Ra	10^3	5×10^3	10^4	5×10^4	10^5	5×10^5	10^6
$Pr = 0.7$							
$HR = RR$	3.4	3.2	2.8	2.2	2.0	1.8	1.8
$\overline{Nu}_{max}$	1.03188	1.28816	1.50114	2.19869	2.57971	3.66347	4.26997

value is reached, mitigating decreases. When compared with that at fixed values of HR and RR, it is remarkable that the average Nusselt number increases as the Rayleigh number increases for over all values of HR and RR. These are to be expected, since the magnitude of buoyant force and hence the strength of the convective cells increases with Ra.

The circumferentially averaged Nusselt number is defined in Eq. (16). A steady state values obtained in the present study are given in Table 2, for various Rayleigh numbers in the four geometry structures under consideration. As the Rayleigh number increases beyond the conduction regime, the curves beyond the pseudo-conduction region are straight lines on log-log coordinates. ($\overline{Nu}$) can be correlated via a least square regression analysis in the form

$$\overline{Nu} = C(Ra)^M \tag{18}$$

For $Pr = 0.7$, where the constant values of C and M are listed in Table 3 for the four configurations considered here.

Average Nusselt number ($\overline{Nu}$) vs. Rayleigh number (Ra) is plotted in Fig. 10. When compared to the different height and radius ratios, it reveals that the ratio of $HR = RR = 2.0$ has largest average Nusselt number at the mid-high Rayleigh number, i.e., ($5.0 \times 10^4 \leqslant Ra \leqslant 10^6$). This configuration implies that the thermal convective heat transfer has a best and optimum space. When the ratio is $HR = RR = 1.2$, the average Nusselt number has smaller value at the overall Rayleigh number. Within such geometry provides least favored circumstance for development of natural convection, but the value of maximum stream function of a narrow gap ($HR = RR = 1.2$) is larger than that of a spacious gap ($HR = RR = 5.0$). This is apparent when we compared it with Figs. 3–5, respectively, which shows that at fixed Rayleigh number, as the height and radius ratios increase, the maximum stream function will be reduced, which is examined in Table 4. However, the influence of height and radius ratio should have a best adequate value of ratio that provides the maximum average Nusselt number.

Table 3
Empirical constants and deviations for Eq. (18)

$HR = RR$	C	M	Ra	Maximum deviation (%)
$Pr = 0.7$				
1.2	0.25747	0.17832	10^3–5×10^5	12.07
2.0	0.20597	0.21853	10^3–10^6	8.43
3.6	0.26301	0.18998	10^3–10^6	5.09
5.0	0.30069	0.17016	10^3–10^6	5.53

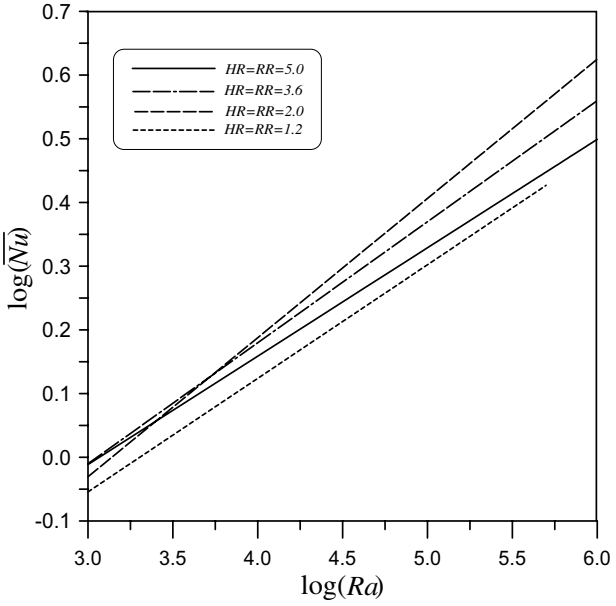

Fig. 10. Average Nusslet number as function of Rayleigh number for $Pr = 0.7$ at four different height and radius ratios.

Table 2
Average Nusselt number

$HR = RR$	$\overline{Nu}$ for Ra						
	10^3	5×10^3	10^4	5×10^4	10^5	5×10^5	10^6
$Pr = 0.7$							
1.2	1.00367	1.12011	1.22905	1.62086	1.93244	3.03176	–
2.0	1.01775	1.23794	1.44840	2.19073	2.57971	3.67983	4.28049
3.6	1.02947	1.28136	1.47159	2.02940	2.32435	3.21156	3.70802
5.0	1.03119	1.23988	1.40425	1.85396	2.09534	2.83389	3.25627

Table 4
Maximum stream function

$HR = RR$	ψ_{max} for Ra						
	10^3	5×10^3	10^4	5×10^4	10^5	5×10^5	10^6
$Pr = 0.7$							
1.2	1.27333	6.26177	10.45337	28.10452	43.52931	105.31536	–
2.0	0.60906	3.03362	5.14669	13.56798	18.70234	23.74348	26.94677
3.6	0.33159	1.62781	2.64004	5.91355	7.63219	10.50863	11.67470
5.0	0.23912	1.17047	1.89283	4.11299	5.26134	7.59035	8.18672

5. Conclusions

The Newtonian fluid between the sphere and vertically cylinder with isothermal boundary conditions has been analyzed numerically by a finite difference method. The steady behaviors of the heat and fluid flow in the annulus have been visualized by means of contour maps of isotherms and streamlines. The numerical results obtained further indicate that heat and fluid flow patterns in the annulus are primarily dependent on the Rayleigh number and the height and radius ratio. The major results may be summarized as follows: (1) at fixed height and radius ratio, the average Nusselt number increases with increase in Rayleigh number; (2) under the situations of the various fixed Rayleigh numbers, the average Nusselt number always increases fast with the increase of the height and radius ratios initially until it reaches has maximum value then it mitigating decreases; (3) the maximum stream function (which the position located on the center of main vortex) decreases with increases in height and radius ratio when the Rayleigh number is unchanged; and (4) the maximum heat transfer is dependent of the height and radius ratio which provides the best thermal convection gap space under the various different Rayleigh number. The above results of numerical calculations can be applied to the realistic case of solar fluid heater. The thermal energy storage may be designed in the optimum ratio of geometry. It will obtain the best thermal energy storage performance.

References

[1] A.W. Date, Numerical prediction of natural convection heat transfer in horizontal annulus, Int. J. Heat Mass Transfer 29 (1986) 1457–1464.

[2] U. Projahn, H. Rieger, H. Beer, Numerical analysis of laminar natural convection between concentric and eccentric cylinders, Numer. Heat Transfer 4 (1981) 131–146.

[3] C. Shu, K.S. Yeo, Q. Yao, An efficient approach to simulate natural convection in arbitrarily eccentric annuli by vorticity-stream function formulation, Numer. Heat Transfer A 38 (7) (2000) 739–756.

[4] C.Y. Han, S.W. Baek, Natural convection phenomena affected by radiation in concentric and eccentric horizontal cylindrical annuli, Numer. Heat Transfer A 36 (5) (1999) 473–488.

[5] J.D. Chung, C.-J. Kim, H. Yoo, J.S. Lee, Numerical investigation on the bifurcative natural convection in a horizontal concentric annulus, Numer. Heat Transfer A 36 (3) (1999) 291–307.

[6] G. Guj, F. Stella, Natural convection in horizontal eccentric annuli: numerical study, Numer. Heat Transfer A 27 (1) (1995) 89–105.

[7] Joo-Sik Yoo, Chol Jun Young, Moon-Uhn Kim, Multicellular natural convection of a low prandtl number fluid between horizontal concentric cylinders, Numer. Heat Transfer A 25 (1) (1994) 103–115.

[8] E.H. Bishop, L.R. Mack, J.A. Scanlan, Heat transfer by natural convection between concentric spheres, Int. J. Heat Mass Transfer 9 (1966) 649–662.

[9] J.A. Scanlan, E.H. Bishop, R.E. Powe, Natural convection heat transfer between concentric spheres, Int. J. Heat Mass Transfer 13 (1970) 1857–1872.

[10] S.H. Yin, J.A. Powe, J.A. Scanlan, E.H. Bishop, Natural convection flow patterns in spherical annui, Int. J. Heat Mass Transfer 16 (1973) 1785–1795.

[11] L.R. Mack, H.C. Hardee, Natural convection between concentric spheres at low Rayleigh numbers, Int. J. Heat Mass Transfer 11 (1968) 387–396.

[12] S.N. Singh, J. Chen, Numerical solution for free convection between concentric spheres at moderate Grashof numbers, Numer. Heat Transfer 3 (1980) 441–459.

[13] K.N. Astill, H. Leong, R. Martorana, A numerical solution for natural convection in concentric spherical annuli, in: Proceedings of the 19th National Heat Transfer Conference, vol. 8, 1980, pp. 105–113.

[14] V.K. Garg, Natural convection between concentric spheres, Int. J. Heat Mass Transfer 35 (1992) 1935–1945.

[15] T. Fujii, T. Honda, M. Fujii, A numerical analysis of laminar free convection around an isothermal sphere: finite-difference solution of the full Navier–Stokes and energy equations between of concentric spheres, Numer. Heat Transfer 7 (1984) 103–111.

[16] M. Fujii, H. Takamatsu, T. Fujii, A numerical analysis of free convection around and isothermal sphere (effects of space and Prandtl number), in: Proceedings of 1987 ASME-JSME Thermal Engineering Joint Conference, vol. 4, 1987, pp. 55–60.

[17] H. Ozoe, K. Fujii, T. Shibata, H. Kuriyama, S.W. Churchill, Three-dimensional numerical analysis of natural convection in a spherical annulus, Numer. Heat Transfer 8 (1985) 383–406.

[18] H. Ozoe, H. Kuriyama, A. Takami, Transient natural convection in a spherical and a hemispherical enclosure, IN: Proceedings of 1987 ASME-JSME Thermal Engineering Joint Conference, vol. 4, 1987, pp. 19–25.

[19] Y. Mochimaru, Transient Natural convection heat transfer in a spherical cavity, Heat Transfer Jap. Res. 18 (1989) 9–19.

[20] H.S. Chu, T.S. Lee, Transient natural convection heat transfer between concentric spheres, Int. J. Heat Mass Transfer 36 (1993) 3159–3170.

[21] C.P. Chiu, W.R. Chen, Transient natural convection heat transfer between concentric and vertically eccentric spheres, Int. J. Heat Mass Transfer 39 (1996) 1439–1452.

[22] C.P. Chiu, W.R. Chen, Transient natural convection between concentric and vertically eccentric spheres with mixed boundary conditions, Heat Mass Transfer 31 (1996) 137–143.

[23] W.R. Chen, Numerical study of thermal wall boundary effects for transient natural convection between concentric and vertically eccentric spheres, Numer. Heat Transfer A 44 (2003) 443–449.

[24] M.A.I. Ei-Shaarawi, A.A.A. Negm, Conjugate natural convection heat transfer in an open-ended vertical concentric annulus, Numer. Heat Transfer A 36 (6) (1999) 639–655.

[25] A. Hadjadj, M. El kyal, Effect of two sinusoidal protuberances on natural convection in a vertical concentric annulus, Numer. Heat Transfer A 36 (3) (1999) 273–289.
[26] F. Moukalled, H. Diab, Laminar natural convection in a horizontal rhombic annulus, Numer. Heat Transfer A 24 (1) (1993) 89–107.
[27] M. Yang, W.Q. Tao, Numerical study of natural convection heat transfer in a cylindrical envelope with internal concentric slotted hollow cylinder, Numer. Heat Transfer A 22 (3) (1992) 289–305.
[28] Y.L. Wu, C. Shu, H.Q. Chen, N. Zhao, Radial basis function-enhanced domain-free discretization method and its applications, Numer. Heat Transfer B 46 (3) (2004) 269–282.
[29] D.A. Anderson, J.C. Tannehill, R.H. Pletcher, Computational Fluid Mechanics and Heat Transfer, Hemisphere, Washington, DC, 1984.
[30] G.E. Schneider, M. Zedan, A modified strongly implicit procedure for the numerical solution of field problems, Numer. Heat Transfer 4 (1981) 1–19.
[31] F. Shahraki, Modeling of buoyancy-driven flow and heat transfer for air in a horizontal annulus: effects of vertical eccentricity and temperature-dependent properties, Numer. Heat Transfer A 42 (6) (2002) 603–621.